Biophysical Reports

ARTICLE

Dominant geometrical factors of collective cell migration in flexible 3D gelatin tube structures

Mitsuru Sentoku,[1] Kento Iida,[1] Hiromichi Hashimoto,[1] and Kenji Yasuda[1,2,*]

[1]Department of Pure and Applied Physics, Graduate School of Advanced Science and Engineering, Waseda University, Shinjuku, Tokyo, Japan and [2]Department of Physics, School of Advanced Science and Engineering, Waseda University, Shinjuku, Tokyo, Japan

ABSTRACT Collective cell migration is a dynamic and interactive behavior of cell cohorts essential for diverse physiological developments in living organisms. Recent studies have revealed the importance of three-dimensional (3D) topographical confinements to regulate the migration modes of cell cohorts in tubular confinement. However, conventional in vitro assays fail to observe cells' behavior in response to 3D structural changes, which is necessary for examining the geometric regulation factors of collective migration. Here, we introduce a newly developed assay for fabricating flexible 3D structures of capillary microtunnels to examine the behavior of vascular endothelial cells (ECs) as they progress through the successive transition across wide or narrow tube structures. The microtunnels with altered diameters were formed inside gelatin-gel blocks by photo-thermal etching with micrometer-sized spot heating of the focused infrared laser absorption. The ECs migrated and spread two-dimensionally on the inner surface of gelatin capillary microtunnels as a monolayer instead of filling the entire capillary. In the straight cylindrical topographical constraint, leading ECs exhibited no apparent diameter dependence for the maximum peak migration velocity. However, widening the diameter in the narrow-wide structures caused a decrease in migration velocity following in direct proportion to the diameter increase ratio, whereas narrowing the diameter in wide-narrow microtunnels increased the speed without obvious correlation between velocity change and diameter change. The results demonstrated the ability of the newly developed flexible 3D gelatin tube structures for collective cell migration, and the findings provide insights into the dominant geometric factor of the emerging migratory modes for endothelial migration as asymmetric fluid flow-like behavior in the borderless cylindrical cell sheets.

SIGNIFICANCE Exploiting our originally developed photo-thermal gelatin-gel three-dimensional (3D) microstructure technology, the dominant rule of collective cell migration for the geometrical aspect in the flexible 3D wide-narrow-wide tubular confinements was examined. The results revealed widening the inner diameter of the capillary tube changed collective migration velocity, following in direct proportion to the diameter change ratio as fluid flow-like behavior. Narrowing of the diameter caused an acceleration of migration speed, whereas no significant correlation between velocity change and diameter change was observed. The potential of the flexible 3D gelatin tube structure method was demonstrated, and the asymmetric dominant geometrical factor of the emerging migratory modes for epithelial cells in 3D structures was suggested.

INTRODUCTION

Collective cell migration is caused by the complex biochemical regulations among component cells in the cell sheet (1–3); however, their dynamics have also been thought to be an emerging fluid flow-like event of cell groups gathered in the confined geometry of our body as the collective motion of active matter (4–7). Such fluid flow-like behavior of collective cell migration contributes to various physiological events, such as the development of embryos (1,8,9), healing of wounds (10), tissue repair (11,12), and blood vessel formation (13), and also drives devastating pathological events, including the invasion of cancer cells into healthy tissues (14). The diverse physiological developments in living organisms involve the intricate coordination between the epithelial cells, which constitute dynamic layers enclosing the surfaces of organs and blood vessels (15,16). To enable the formation of these

Submitted July 5, 2022, and accepted for publication July 15, 2022.

*Correspondence: yasuda@list.waseda.jp

Mitsuru Sentoku and Kento Iida contributed equally to this work.

Editor: Jorg Enderlein.

https://doi.org/10.1016/j.bpr.2022.100063

© 2022 The Author(s).

This is an open access article under the CC BY-NC-ND license (http://creativecommons.org/licenses/by-nc-nd/4.0/).

diverse structures, epithelial cells and endothelial cells (ECs) exist in different modes of coordinated migration, including sheets for wound healing, ducts for blood vessel networks, strands, and clusters (17,18). These collective cell behaviors are essential in maintaining proper biological functions, and any dysfunction during the process can incur physical concerns such as developmental defects and tumor metastasis. Studying the migration behavior of collective cells under environmental constraints is important in identifying the external factors governing the cellular morphology that underlies physiological functions crucial for promoting disease therapies. Therefore, the ability and limitations of a fluid flow-like model used to explain the coordinated behavior of collective cell migration should be examined to generalize those events.

The contribution of geometric confinement structures has been extensively studied in many groups as one of the dominant factors of collective cell migration to examine the emerging fluid flow-like behavior of collective cell migration (19,20). For example, a positive effect of geometric curvature in the three-dimensional (3D)-engineered polydimethylsiloxane (PDMS) tortuous microchannels on the collective cell migration velocity was reported (21). The role of local geometry such as substrate surface curvature for the organization, migration, detachment, and growth rate of individual cells in the sheet was also reported (22). The results explained an apparent correlation between curvature and cell growth. However, those results did not support the diameter dependence of collective migration velocity in 3D tubular structures. Even at the single-cell level, the geometry of confinement structures affects the dynamics of single cells (23). Adding to the studies on the large-scale geometric confinement structures, the importance of micrometer-sized structures on a two-dimensional (2D) substrate was also reported as its topographic control of directed cell migration (24). The formation of a curved epithelial monolayer enclosing the central cavity in the 3D confinement is also one of the unique characteristics of collective cell migration because the border does not exist in the sheets, and practically these shapes are essential to form the body structures (22). For example, by combining experimental measurements and computational modeling, the geometric dependence of 3D collective cancer invasion was coordinated by the mechanical feedback between individual cells and their surrounding extracellular matrix (ECM) (25). Moreover, observation of tumor cell migration through confining tracks in vivo showed that their behavior was not predicted by the 2D model (26). However, in contrast to the 2D studies on flat substrates, the 3D research of fluid flow-like behavior in collective migration has not been examined sufficiently because of the difficulty in preparing a flexible 3D platform for assessing cellular dynamics.

Recent studies in collective cell migration have attempted to feature a 3D culturing environment to investigate the dynamics of endothelial and epithelial cell sheets during lumen formation. In vitro spontaneous self-construction of blood vessel-like capillary tubes from cultured ECs were well known and reported from 1980s (27). The earliest studies of 3D culturing assays also elicit tubulogenesis of epithelial cells by culturing inside collagen matrices with fibroblasts (28,29). Because the guiding path is absent from this type of culturing method, the branching direction is unregulated, making this culturing assay unsuited for studying the cell dynamics. To investigate the influence of out-of-plane curvature on the migration of cell cohorts, studies have observed the formation of tubular cell assembly surrounding a glass rod with a diameter as small as 1 μm (30,31). While the methodology employed in these studies allowed strictly controlled diameter sizes on which the cells were seeded, the cylindrical tissue formed by the cells on the periphery resulted in inverted polarity, which is inherently different from the known in vivo structures. In a more recent study attempting to mimic the luminal conformation of epithelial cells by creating microtube platforms, the dynamics of coordinated cell migration for tubes with different diameters were considered (32). However, vessels do not maintain a constant diameter, and collective cell response to topography changes in microtubular structure has yet to be observed.

A significant limitation preventing this type of study was the difficulty in preparing the extracellular matrix with structures other than a simple straight tunnel. An investigation was done to investigate the effects of arterial thrombosis by constructing a 3D printed microfluidic vessel. However, the minimum diameter available by this technique was 100 μm, and any value below this limit resulted in a fragile microvessel or a collapse during the fabrication process. Moreover, this investigation focused on computing the blood perfusio inside the 3D printed vessel, and no direct insight was given into the dynamics of the cells adhering to the inner walls (33).

To unveil the dynamics of cell cohorts and the effects induced by spatially restricted in vivo scenarios on the migration phenomenon, we have developed a non-lithographic approach for the preparation of a 3D culturing environment containing microconfinements inside a gelatin-gel block. The photo-thermal 3D gelatin-gel microfabrication technology is accomplished by utilizing the laser-focused microneedle implemented on a device capable of adjusting the laser intensity and the position of the gelatin-gel block, allowing flexible microtubes with a diameter as small as a single cell to be

fabricated on the lateral wall of the gel. Exploiting this technology, we examined the dominant geometric rule of collective motion in the borderless endothelial cell sheet enclosed in a seamless cylindrical shape that does not have the edges of a cell sheet observed in the conventional 2D platforms. The flexible change of diameters in wide-narrow, narrow-wide, and wide-narrow-wide microtunnel structures were fabricated in gelatin-gel blocks. The underlying rule was investigated by comparing the propagation velocity change and the circumference length change in a microtunnel. Furthermore, we observed the change in the front edge cells of the propagating cylindrical cell layer when the cohort encountered abrupt topographical changes in the single-cell-sized pinhole wide-narrow-wide structure.

MATERIALS AND METHODS

Cells

We used a mouse-derived endothelium-like cell line (MILE SVEN 1 (MS1); CRL-2279, ATCC, Manassas, VA, USA) in this experiment. The cells were grown at 37°C under 5% CO_2 in Dulbecco's modified Eagle's medium (DMEM; Gibco, Thermo Fisher Scientific, Waltham, MA, USA) supplemented with 10% heat-inactivated fetal bovine serum (FBS; Gibco, Thermo Fisher Scientific, Waltham, MA, USA) and 100 U /mL penicillin-streptomycin (Gibco, Thermo Fisher Scientific, Waltham, MA, USA).

Production of glass microneedle

The base material of the microneedle used for 3D microfabrication was the borosilicate glass capillary tubes with internal glass fiber (GD-1, NARISHIGE, Tokyo, Japan). Microneedles were fabricated by elongating the capillary tube with a puller (PC-100, NARISHIGE, Tokyo, Japan) set at heater setting 70. This process produced a sharp endpoint of only several micrometers, which is then heated with microforge (MF-900, NARISHIGE, Tokyo, Japan) to fabricate a spherical designated diameter. Furthermore, as the needle is stationed at an angle to the petri dish containing gelatin substrate, the end region of the microneedle must be angled to become parallel to the microscope stage for fabrication of microtunnels. This is also accomplished by heating approximately 5 mm away from the endpoint using microforge. The glass tip was coated with platinum by vapor sputtering under Auto Fine Coater (JFC-1600, JEOL, Tokyo, Japan) manually set at 30 mA current for 120 s duration.

A focused 1064-nm infrared laser irradiation setup

A 1064-nm infrared laser irradiation setup consists of the following three major parts: a phase-contrast microscope (IX-71, Olympus, Tokyo, Japan) with a motorized XY stage (BIOS-206T, SIGMA KOKI, Tokyo, Japan), a 1064-nm infrared laser (PYL-1-1064-M, IPG Laser, Burbach, Germany), and a glass microneedle fixed in a 3D micromanipulator (MHW-3, NARISHIGE, Tokyo, Japan).

Gelatin-gel cube preparation

The gelatin (derived from bovine skin type B, Sigma-Aldrich, St. Louis, MO, USA) was mixed with purified water to create a concentration of 1.8% (w/v) gel. The mixture was heated inside the water bath set at 37°C. After mixing the gelatin gel, the mixture was moved to a 35-mm petri dish that was solidified inside a refrigerator.

Microfabrication of 3D structures in gelatin gel

A 6-mm (width) $\times$ 6-mm (depth) $\times$ 4-mm (height) cube of 1.8% (w/v) gelatin gel was prepared for microfabrication. A portion of gelatin gel was solated by the spot heating of the microneedle tip with the absorption of the focused 1064-nm infrared laser. The motorized XY stage was moved at about 11 μm/s during the microfabrication process.With the control of the position of the end of the microneedle and the intensity of the infrared laser, flexible 3D confinement was fabricated inside the gelatin gel. After constructing the structures, crosslinking was performed by immersing the gelatin gel inside 10% glutaraldehyde (FUJIFILM Wako Pure Chemical, Osaka, Japan) for 30 min and then washed with ample purified water. Finally, the crosslinked gelatin cube was immersed in DMEM, and MS-1 cells were seeded onto the gelatin cube for observation inside the microtunnel.

Cell cultivation in gelatin-gel microstructures

A gelatin cube was set in the 35-mm cultivation dish (3000-035, AGC TECHNO GLASS, Shizuoka, Japan) filled with DMEM-buffer and 3×10^4 cells MS-1 cells were placed on the cultivation dish and incubated at 37°C under 5% CO_2. Then, the adhered MS-1 cells proliferated on the surface of gelatin cube and migrated into the microstructures. The progression of the cellular assembly was observed by time-lapse observation using a charge-coupled device (CCD) camera (CytoWatcher WSL-1800, ATTO, Tokyo, Japan).

Time-lapse recording and analysis of cellular dynamics

Time-lapse 10-minute-interval images of the cells inside the topographical constraints were taken by CytoWatcher. From the obtained time-lapse images, the front cells or the observable leading edges were tracked by utilizing the MtrackJ plugin of the Java language-based image processing program ImageJ (NIH, Bethesda, MD, USA). As for the tracking of cell migration inside 3D tubular structures, continuous analysis was obscured by occasional cylindrical motion that allowed a different cell to appear as the leading edge. In such cases, the fluctuating measurement is treated as an outlier, and tracking is resumed from the front cell. By manually tracking the upper and lower positions of the cells for image slices of 1-h intervals, the displacements and migration velocities of the collective cellular flow inside 3D confinement were measured.

Confocal cross-sectional imaging of cells

Cross-sectional images of cells in the microtunnels were acquired with confocal microscopy (FLUOVIEW, Olympus, Tokyo, Japan). For the fluorescence imaging, the cells in the gelatin microstructure were stained with staining dye, calcein AM (endothelial tube formation assay (in vitro angiogenesis), Cell Biolabs, San Diego, CA, USA). The staining process was conducted by washing the cells with a 9:1 ratio of staining solution and DMEM-buffer and placing it inside the incubator for 30 min. The solution was then removed, and the staining dye (diluted with the earlier solution) was added to the culture dish. After letting the staining proceed for 60 min, the cells were washed thoroughly with DMEM (phenol red (−), 1% FBS), and images were obtained with the confocal microscope.

Statistical analysis

All statistical values of propagation velocities are presented as mean ± standard deviation (SD) of 10-min interval recorded propagation velocities (unless stated otherwise). The result of fitting linear equations to a set of data points was performed using ordinary least-squares regression (OLS) in Microsoft Excel (Microsoft, Redmond, WA, USA). Correlation coefficient of data was also acquired with Microsoft Excel. The normality of the acquired data was evaluated by the Shapiro-Wilk test. These propagation velocities were also evaluated using the non-parametric Mann-Whitney U test or F test and following t test. $p < 0.05$ was considered statistically significant. Shapiro-Wilk test, U test, F test, and t test were performed using R (R Foundation for Statistical Computing, Vienna, Austria).

RESULTS

Fabrication of flexible 3D tubular tunnels in gelatin gel for collective cell migration measurement

To understand the dynamics of vascular endothelial cells (ECs) in angiogenesis in flexible 3D confined environments, we have developed a novel method to fabricate the flexible capillary microtunnels in gelatin gel. The developed on-chip photo-thermal 3D gelatin-gel microfabrication system is described as follows: the design of the system setup is illustrated in Fig. 1 *A*. The two major components of this system are the focused permeable 1064-nm infrared laser, which is permeable to water, for spot heating on the platinum-coated microneedle tip and the motorized XY stage. By manipulating the laser intensity, micrometer-sized spot heating is allowed by the laser absorbance, which induces heat for melting the surrounding portion of gelatin gel. The gelatin gel used throughout the investigation was set at 1.8% concentration for optimal balance between cell adhesion and ease of microfabrication. The motorized XY stage is employed to provide the user control over the location of the gelatin piece during the process of microfabrication.

A more elaborate explanation of the microfabrication process is described in Fig. 1 *B*. As shown in the schematical drawing, the tip of the glass microneedle was modified to form the spherical shape to fabricate stable microstructures. The principle of this fabrication procedure is as follows: the absorption of the focused 1064-nm infrared laser beam at the platinum-coated microneedle causes the tip of the microneedle to generate the heat necessary to melt the surrounding areas of the gelatin gel (a). The 3D position of the microneedle tip was controlled flexibly by the micromanipulator during microfabrication. Then, 3D microstructures were fabricated from the lateral side of the gelatin gel by maneuvering the motorized XY stage so that the gelatin gel approaches the spot-heated microneedle tip (b). As the gelatin gel progresses over the laser-focused microneedle, the generated spot heat constructs the tubular structure inside the gel through which the epithelial cells can migrate.

The series of micrographs displayed in Fig. 1 *C* exemplify the actual microfabrication process of generating a 300-μm tunnel into a gelatin-gel block from the left lateral surface. As the gelatin gel approached the microneedle from the right side (a) with a gradual movement of the motorized XY stage, the surrounding area of the microneedle melted (b), and the microtunnel was formed (c and d). An illustration with more details of Fig. 1 *C*(d) is given schematically by Fig. 1 *D* delineating the process of tunnel formation at the melting area inside the gelatin gel. The heat is induced by the spot focusing of a 1064-nm infrared laser on the platinum-coated microneedle tip, forming the tunnel. The melted portion of gelatin gel was solated and dispersed into the surrounding water, which the gelatin gel was placed inside.

The inner diameter of the microtubular structure can be controlled by changing the laser power. Examples of microtubular structures with varying inner diameters are represented in the phase-contrast images (Fig. 1 *E*). By utilizing different irradiation laser powers, microtunnels of 23 μm for 5 mW (a), 58 μm for 7 mW (b), 83 μm for 9 mW (c), and 132 μm for 13 mW (d) were microfabricated, respectively. The correlation between the laser power and the inner diameter was obtained by plotting the utilized laser power and the fabricated microtubular structures Fig. 1 *F*. The emission power of the infrared laser was measured using the power meter (FM 33-0506, Coherent, Santa Clara, CA, USA). As demonstrated by the graph, the system exhibited a linear correlation between the inside diameter of microtunnels and the laser power. In addition, the inside diameter of the microtunnels can also be regulated by modifying other parameters, such as the diameter of the microneedle's tip (e.g., a thinner tip can form a smaller tunnel), the material used for vaporized deposition (e.g., higher absorbance can require lower laser intensity), and the speed at which the microscope stage maneuvers the gelatin piece towards the stationary needle for construction of the microtunnel. As a result of combining these parameters, we confirmed that the range of the inside diameter of microtunnels was from 20 to 350 μm in this setup.

This developed technology utilizing photo-thermal etching permitted the fabrication of flexible widths in straight tunnels without using the mold for conventional cast-mold methods, which can only form simple linear shapes of tunnels. In detail, multiple 3D width designs can be manufactured by adjusting the laser power during the fabrication process of a straight tunnel inside gelatin gel. In Fig. 1 *G*, examples of 3D structures that were created through this developed microfabrication system are displayed. A microtubular structure of

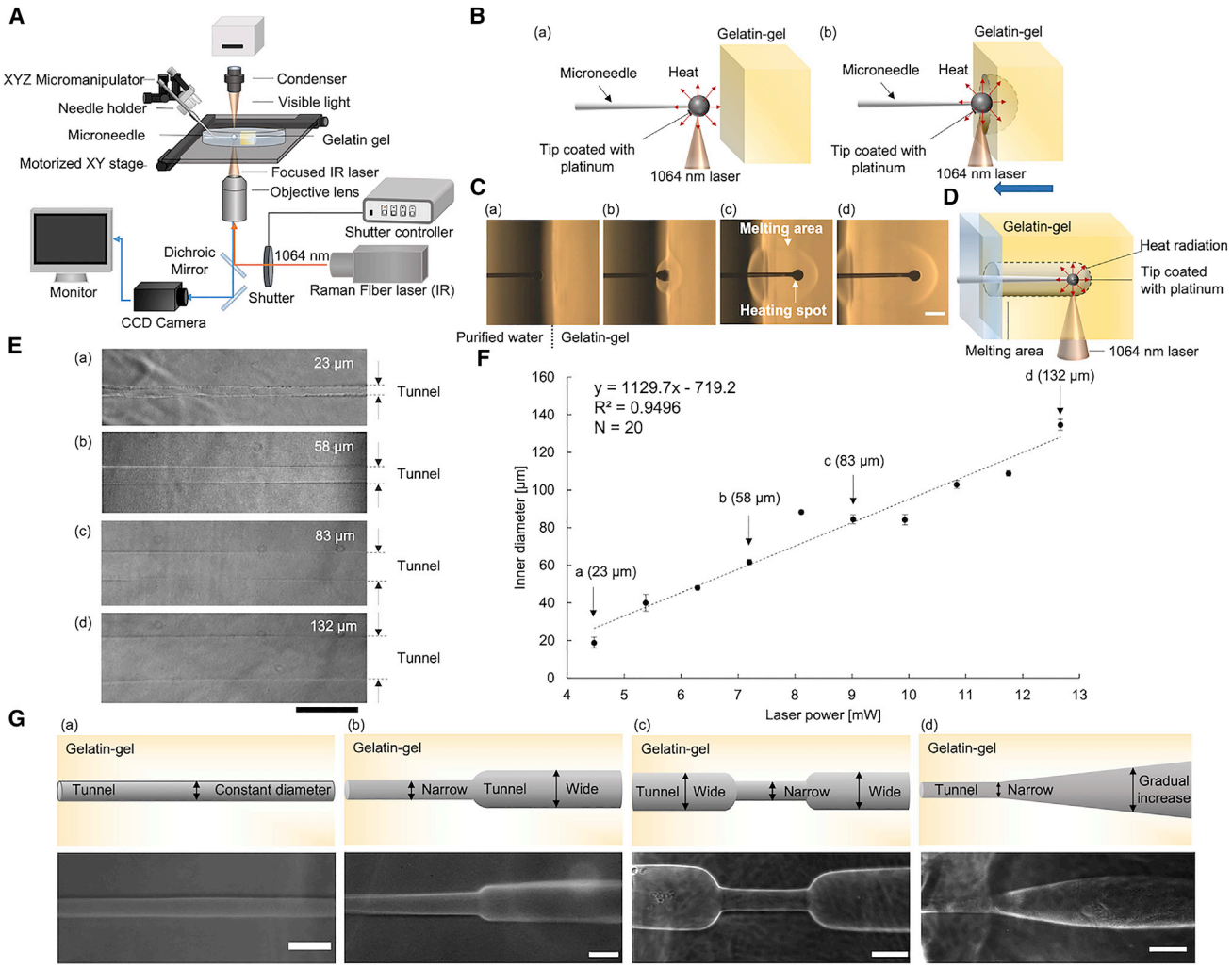

FIGURE 1 Design and performance of the on-chip photo-thermal three-dimensional (3D) gelatin-gel microfabrication system. (*A*) Schematic diagram of the system setup. The two main technologies adopted that allow precise construction of a flexible tubular structure consist of the motorized XY stage and the permeable 1064 infrared laser for spot heating of the absorbance tip of the microneedle. (*B*) Illustration of the process of gelatin microfabrication. The gelatin gel placed on the motorized XY stage is controlled to gradually approach the platinum-coated spherical-shaped tip (heating spot) of the microneedle ((a) and (b)). (*C*) A series of micrographs during the process of microtunnel formation of a 300-μm tunnel inside gelatin gel; (a) before melting, (b) start of the melting process at the boundary of the gelatin gel, (c) and (d) formation of the tunnel by the movement of the gelatin gel on the motorized XY stage. Bar, 100 μm. (*D*) Schematic illustration of (*C*) (d) representing the process of generating a tunnel at the melting area inside the gelatin gel. By controlling the irradiation intensity of the focused 1064-nm infrared laser, the temperature of the heating spot can be regulated. Therefore, the inner diameter of the microtunnel can be adjusted according to the user's interest. (*E*) Phase-contrast images of microfabricated tunnels with different laser irradiation powers. Microtunnels of 23 μm (a), 58 μm (b), 83 μm (c), and 132 μm (d) were created with the laser power of 5 mW, 7 mW, 9 mW, and 13 mW, respectively. (*F*) Correlation demonstrating the laser intensity and the tunnel inner diameter generated with a platinum-coated microneedle. SD, fluctuation of inner diameter (N = 20). (*G*) Examples of various microtunnel structures produced by altering the irradiation laser power during the tunnel formation process: (a) straight width tunnel (no laser power change); (b) narrow to wide (low power to high power); (c) wide-narrow-wide (high-low-high); (d) gradual narrow (gradually increasing the laser power). Phase-contrast images of microstructure illustrations are represented below. Bars, 100 μm.

constant inner diameter was generated similar to that of previously conducted research with cast-mold methods (Fig. 1 *G*(a)). On the other hand, our flexible 3D designs where the inside diameter of the microtunnel sharply shifts from narrow to wide (Fig. 1 *G*(b)), wide-narrow-wide (Fig. 1 *G*(c)), and also gradual change from narrow to wide (Fig. 1 *G*(d)) were produced to further investigate the fluid flow-like behaviors of the migrating epithelial sheet. The other forms associated with diameter changes during the microfabrication process demonstrate the flexible width control enabled by this developed gelatin-gel fabrication device, which was challenging to construct prior to this technology. By adjusting the laser power accordingly while moving the XY stage, a structure of interest with the desired diameter can be created.

Exploiting this technology, we cultivated pancreatic islet-derived MILE SVEN 1 ECs (MS-1) in a straight cylindrical microtube fabricated in the gelatin block. In the beginning, the source of migrating MS-1 cells was precultivated on the outer surface of the gelatin block. After the cells proliferated and reached the entrance of the microtube, the MS-1 migrated into the 54-μm-diameter microtunnel spontaneously and extended the entire inner surface of the microtunnel as shown in Fig. 2 *A*. In this example, 10 h after observation started, the migration velocity of front edge cells was 7 μm/h just close to the entrance of microtunnel (Fig. 2 *A*(a)). Then, the propagation velocity of front edge cells increased and reached to maximum peak velocity (19 μm/h) 15 h after observation started (Fig. 2 *A*(b)). However, after reaching the maximum peak velocity, the migration gradually decreased monotonously according to the propagation distance from the cell reservoir (Fig. 2 *A*(c), 30 h after observation started). As shown in those micrographs, leader cells in the microtunnel protruded from the cell front, drawing rows of follower cells after them while maintaining 2D structures. Similar collective cell migration behavior in 2D flat sheets were reported in the previous papers (6,34–38). Fig. 2 *B* represents the phase-contrast (a) and confocal cross-sectional (b) images of migrated cells in the microtunnel. As shown in the longitudinal cross-sectional fluorescence image, the calcein-stained cells were attached only to the inner surface of the gelatin-gel tunnel and migrated two-dimensionally in the microtunnel. The time-course

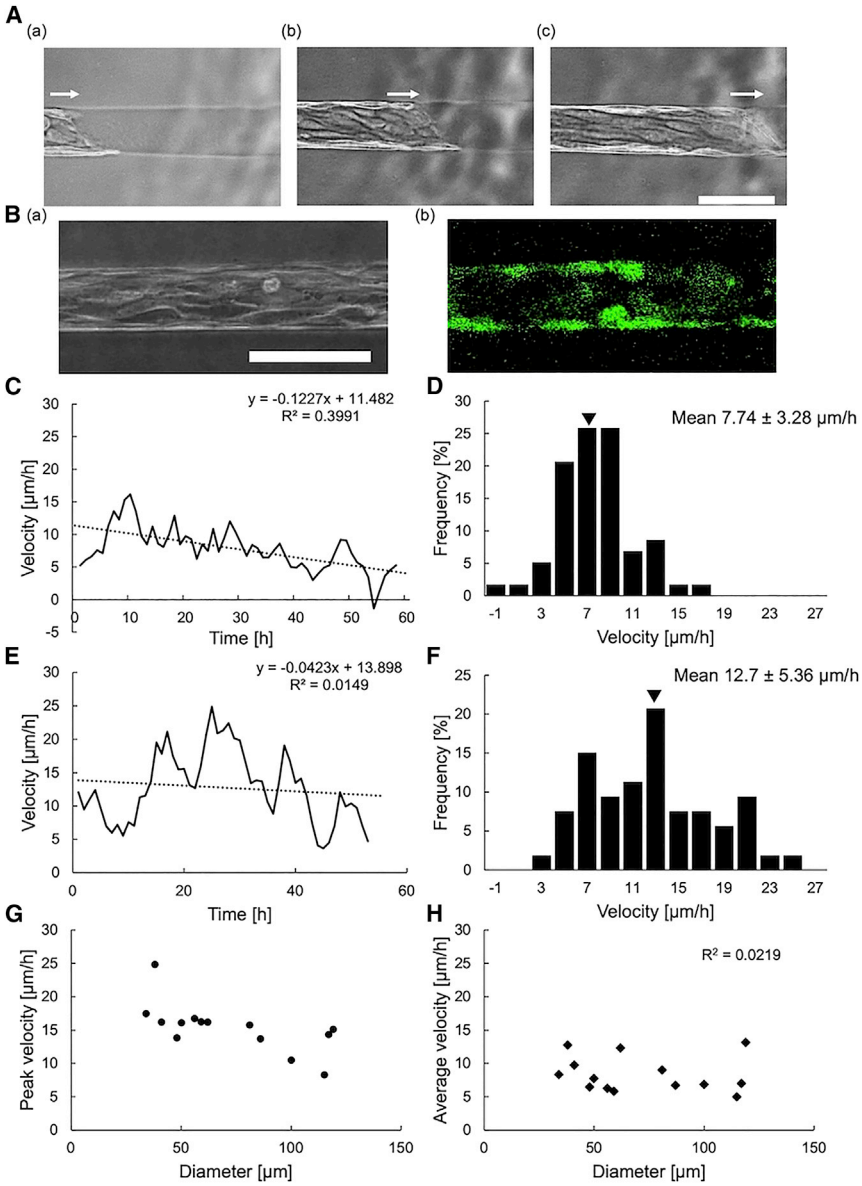

FIGURE 2 Obtained time-lapse imaging of the collective cell migration on the inner peripheral surface of the generated 3D microtunnel and the associated velocity analysis of the cell tracking on the image slices. (*A*) The bright-field images of the collective cell migration into the 54-μm straight capillary microtunnel structure (a) before cell migration started, (b) 3 h after cell migration started, and (c) 10 h after cell migration started. Bar, 100 μm. (*B*) Phase-contrast (a) and confocal cross-sectional (b) images of migrated cells in the microtunnel of sample (*A*). The cells were stained by calcein. Bar, 100 μm. (*C*) Temporal analysis of the velocity profile of migration inside 54-μm diameter microtunnel of sample (*A*). In this example, after initial acceleration, a monotonic decay in velocity was observed after long duration of measurement. (*D*) Histogram of migration velocity distribution of sample (*A*). (*E*) Temporal analysis of the velocity profile of migration of another example inside 38-μm diameter microtunnel. In this example, the propagation velocity was fluctuating. (*F*) Histogram of migration velocity distribution of sample (*E*). (*G*) Microtunnel diameter dependence of maximum peak velocity of front edge cells. (*H*) Microtunnel diameter dependence of average velocity of front edge cells. Dashed lines in (*C*) and (*E*) represent the ordinary least-squares regression results of samples.

of collective migration in the straight microtunnel of this sample (Fig. 2 *A* and *B*) is described in Fig. 2 *C* and *D*. In this example, migration velocity increased to the maximum peak velocity of 19 μm/h after entering into the microtunnel from the outer surface and then gradually decreased monotonously to 2 μm/h. Fig. 2 *E* and *F* show one of the other 14 samples in the straight microtubes. Here, the propagation velocity fluctuated with a faster mean migration velocity without apparent decay of propagation velocity. Including these examples, all 14 samples propagated in the gelatin microtunnel structures. However, the propagation manners were varied, and no apparent correlation between microtunnel diameter and propagation velocity was observed, at least in those 14 samples (Fig. 2 *G* for maximum velocity distribution, and Fig. 2 *H* for mean velocity distribution).

As demonstrated above, we confirmed that the gelatin microtubes could work as the platform of collective cell migration observation in 3D capillary microtubes. However, the propagation manner of cells does not seem to correlate to the diameter of microtunnels. Moreover, collective migration velocity also fluctuated among samples. The origin of this fluctuation remains uncertain. Regardless, it may be caused by the cell supply at the entrance of the microtunnels because these fluctuations were not observed in 2D structures on the flat plane, in which the structures were directly connected smoothly and seamlessly with the cell reservoir region on a flat plane. As a consequence, it is necessary to consider the influence of cell supply at the entrance to compare the behavior of collective cell migration among different samples. Furthermore, it implies the difficulty of comparing the difference in migration velocities in various microtunnel diameters using different samples. Even under such a limitation, the flexible change of microtunnel structures can still have the potential to indicate the influence of physical structure changes on the collective cell migration by comparing the change of propagation manners in each part of the flexible structure within a microtunnel as a part of the series events of collective migration of identical samples. Hence, we applied this assay for understanding the contribution of 3D geometrical structure changes to collective migration behaviors during their propagation in flexible widening/narrowing microtunnels.

Tunnel diameter dependence of propagation velocity in flexible changed 3D gelatin-gel structures

In Fig. 1, flexible changes in 3D microtunnel designs with on-chip photo-thermal gelatin-gel microfabrication technology were accomplished for collective cell migration measurements. As demonstrated in Fig. 2, the results of collective cell migration in the straight microtunnels suggested the difficulty of comparing the migration behavior in different microstructures with different samples, which is also enhanced by inlet inconsistencies. Hence, we applied this newly developed technology to form the successive transitions from wide-narrow, narrow-wide, and wide-narrow-wide structures within the same single microtunnels and compared the migration velocity changes caused by the consecutive structural changes.

This assay development aimed to understand the direct contribution of geometric structures to the change of collective cell migration patterns. In other words, our question was how altering the tunnel diameters influences the acceleration/deceleration manner of propagation velocity. In a previous study examining the role of geometrical confinement on collective cell migration on 2D stripe structures, a decrease in the width of the channel was accompanied by an overall increase in the migration velocity (7). Flow field analysis of an unidirectional 2D cell sheet expansion inside confined geometries in a different report also showed that the flow velocity can be decomposed into a constant term of directed cell migration and a diffusion-like contribution, which increases with density gradient (6). If the propagation velocity of collective cell migration in 3D microtunnels is dominated not only by the biological factors and nutrition environment but also by the physical law, such as the continuity equation or Fick's law of diffusion (i.e., $\partial\rho/\partial t + \nabla\cdot\vec{j} = \sigma$, where ρ is the amount of the cells per unit volume or cell density, $\vec{j}$ is the flux of ρ, and σ is the increase of cells per unit volume per unit time), the narrowing of the inner diameter of the tube should accelerate the propagation velocity to satisfy the continuity equation.

In the wide-to-narrow microtunnel, as shown in Fig. 3 *A*, the migration velocity at the front was also accompanied by an overall increase as the cell sheet transitioned into the narrower section. The trace of the two front cells in the front edge cells was plotted in green and blue open circles every 1 h in the micrograph, indicating the cells were migrating straight forward in the microtunnel while maintaining their positions in a radial direction even after sudden narrowing of the microtunnel structure. While the average migration velocity was tracked to be 12.3 μm/h in the wide area (62 μm), the average velocity increased to be around 19.6 μm/h after entering the narrow area (32 μm), which is given by the velocity-time graph in Fig. 3 *D*. The histograms of Fig. 3 *G* and *H* represents the frequency analysis of the wide and narrow sections, respectively. The corresponding histograms further demonstrate that the overall velocity exhibited by the collective cell migration increased after entering the narrower section of the microtunnel. Thus, the wide-narrow microtunnel

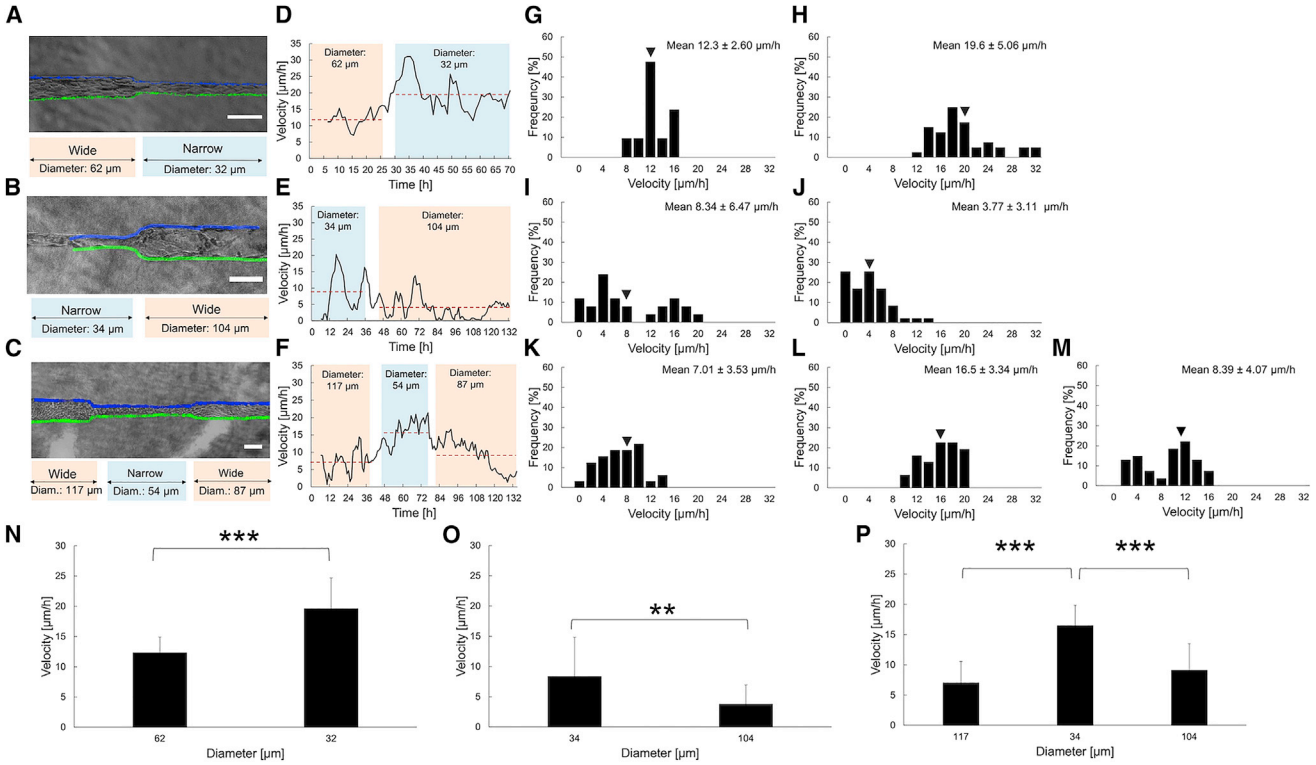

FIGURE 3 Obtained time-lapse imaging of the collective cell migration on the inner peripheral surface of the various 3D microstructures and the associated velocity analysis of the cell tracking on the image slices. (*A*–*C*) The phase-contrast images of the collective cell migration inside different microtunnel structures; namely, (*A*) wide-narrow change from 62 to 32 μm during 30-μm length, (*B*) narrow-wide change from 34 to 104 μm during 20-μm length, and (*C*) wide-narrow-wide change from 117 to 54 μm in 20-μm length and to 87 μm in 50 μm length. The green and blue open circles correspond to the tracked location of specific cells for 1-h interval represented by the phase-contrast image of each structures. Bars, 100 μm (*D*–*F*) Time course of migration velocity in various structures; (*D*) wide-narrow (mean velocities, 12.3 ± 2.60 μm/h, 19.6 ± 5.06 μm/h, respectively), (*E*) narrow-wide (mean velocities, 8.34 ± 6.47 μm/h, 3.77 ± 3.11 μm/h, respectively), (*F*) wide-narrow-wide (mean velocities, 7.01 ± 3.53 μm/h, 16.5 ± 3.34 μm/h, 8.39 ± 4.07 μm/h, respectively). The errors are the standard deviations of the corresponding mean velocitites. The migration velocity has been determined for the respective microtunnels in each 1-h interval. The green and blue bars on the graphs correspond to the tracked location represented by the phase-contrast image of each structure. Red dashed lines show the mean velocity of each structure. (*G*–*M*) Histograms of velocity distribution in various structures; (*G*) wide part of wide-narrow, (*H*) narrow part of wide-narrow, (*I*) narrow part of narrow-wide, (*J*) wide part of narrow-wide, (*K*) the first narrow part of wide-narrow-wide, (*L*) wide part of wide-narrow-wide, (*M*) the narrow part of wide-narrow-wide. (*N*–*P*) Significance test of narrow-wide, wide-narrow, wide-narrow-wide width samples of (*A*)–(*C*), respectively. *p < 0.05, **p < 0.01, ***p < 0.001.

exhibited an increase in migration speed as the inner diameter of the structure decreased, indicating the possible influence of cell supply increase by the narrowing structural change.

The narrow-to-wide microtunnel exhibited the opposite behavior, where the migration velocity decreased as the collective cell sheet encountered a sudden increase in structural diameter. An example trial is given in Fig. 3 *B* with its corresponding velocity profile in Fig. 3 *E*. The trace of two front cells also migrated straight forward while maintaining their location in the radial direction even after widening the microtunnel structure. The average velocity tracked in the narrow section (34 μm) was determined to be 8.34 μm/h, whereas it was 3.77 μm/h for the wide area (104 μm). The tendency is further demonstrated in the histograms of the narrow section (Fig. 3 *I*) and the histogram of the wider area (Fig. 3 *J*), as more velocity exhibited lower values than the preceding narrow area. By examining the collective cell migration inside a structure with a sudden increase in inner diameter, the speed reduction of the cell sheet was observed.

The results also showed that even these flexible 3D microtubular confinements could organize cell flows without creating disordered patterns of swirls or active turbulence, which occurs in large tissues (39–41). Even in the 2D stripes, shear flow and transverse flow were observed only in the wider stripes (42). They indicate the circumferences of the borderless cylindrical 3D closed structures can also play the regulatory role during the change of their circumference length, even without edges of those cell sheets.

Finally, to observe whether the collective cell migration inside a more complicated microtubular structure

exhibits similar tendencies, a tunnel was fabricated with successive transitions between wide-to-narrow and narrow-to-wide areas. In the wide-narrow-wide tunnel (Fig. 3 *C*), the three-step consecutive changes in the inner diameter of the microtubular structure caused the collective cell migration velocity to change accordingly as in the previous wide-narrow and narrow-wide tunnels. An example of this type of microtubular structure analysis is provided in Fig. 3 *F*. The trace of two front-end cells also migrated straight forward, maintaining their positions in the radial direction even after the sudden widening and narrowing of microtunnel structures. While the cell sheet was migrating at 7.01 μm/h in the first area with the inner diameter of 117 μm, the migration velocity demonstrated an increase to 16.5 μm when the cell sheet invaded through the narrow section (54 μm) of the tunnel as expected from the previous wide-narrow tunnel. However, the migration velocity was accompanied by a decrease to 8.39 μm/h once the cell sheet progressed into the second wide section with 87-μm diameter. A histogram is given for the examples of wide-narrow-wide tunnel at each section to demonstrate the distribution of migration velocity (Fig. 3 *K–M* for the corresponding wide, narrow, wide sections respectively).

Statistical tests were employed to determine whether the velocities obtained in the different regions of each sample were significantly different. Although there were fluctuations in the migrating velocities, the tests demonstrated that there were significant differences between the corresponding velocities for the samples shown above wide-narrow, narrow-wide, and wide-narrow-wide structures in Fig. 3 *N* ($p < 0.001$), 3O ($p < 0.01$), and 3P (wide-to-narrow part: $p < 0.001$, and narrow-to-wide part: $p < 0.001$) respectively.

Table 1 shows the summary of the wide-narrow, the narrow-wide, and the wide-narrow-wide results in various diameter ratios. Similar to the above results in Fig. 3, the wide-narrow patterns and the wide-narrow section of the wide-narrow-wide patterns showed increases in collective migration velocity as the microtunnel diameter reduced. The narrow-wide structures and narrow-wide section of the wide-narrow-wide patterns also demonstrated decreases in collective migration velocity with widening structural changes. Statistical tests for all these 12 samples were also employed to determine whether the velocities obtained in the different regions of each sample were significantly different. Fig. 4 shows the results of three wide-narrow, three narrow-wide, and six wide-narrow-wide structures. The tests also demonstrated a significant difference between the corresponding velocities for the 12 wide-narrow, narrow-wide, and wide-narrow-wide structures, except for the narrow-wide part of the wide-narrow-wide pattern in Fig. 4 G.

TABLE 1 Comparison of inner diameter and velocity of collective cell migration for different tubular structures

Tubular structure		Inner diameter (μm)	Average velocity (μm/h)	Maximum velocity (μm/h)
Wide-narrow tunnel	wide	62	12.3 ± 2.60	16.2
	narrow	32	19.6 ± 5.06	31.0
	wide	87	7.83 ± 2.60	13.8
	narrow	30	11.8 ± 2.87	16.3
	wide	115	5.01 ± 1.55	8.32
	narrow	40	7.53 ± 2.67	11.2
Narrow-wide tunnel	narrow	34	8.34 ± 6.47	20.3
	wide	104	3.77 ± 3.11	13.8
	narrow	41	9.76 ± 3.15	16.2
	wide	77	6.70 ± 2.48	12.9
	narrow	48	6.48 ± 4.66	13.9
	wide	61	4.01 ± 3.14	12.6
Wide-narrow-wide tunnel	wide	81	9.06 ± 5.19	16.9
	narrow	34	22.2 ± 6.05	28.3
	wide	48	16.5 ± 7.95	27.9
	wide	100	6.89 ± 2.29	10.6
	narrow	41	12.1 ± 3.65	15.9
	wide	89	2.35 ± 1.35	7.11
	wide	110	11.2 ± 1.47	13.2
	narrow	44	17.5 ± 3.91	22.2
	wide	69	13.9 ± 1.30	15.7
	wide	117	7.01 ± 3.53	14.3
	narrow	54	16.5 ± 3.34	20.9
	wide	87	8.39 ± 4.07	14.1
	wide	119	13.2 ± 1.34	15.1
	narrow	46	15.6 ± 4.48	22.6
	wide	96	11.9 ± 2.03	16.0
	wide	159	8.58 ± 3.29	13.4
	narrow	51	20.5 ± 2.88	23.5
	wide	149	4.83 ± 2.12	10.5

The graph in Fig. 5, which plots the Table 1 results, demonstrates the correlation between the relative diameter transitions from D1 (inlet side) to D2 (outlet side) of narrow-wide ($D1/D2 < 1$) or wide-narrow ($D1/D2 > 1$) patterns and the relative migration velocity changes from V1 (inlet side) to V2 (outlet side) of those results (Table 1). As shown in the graph, both the average and maximum peak velocity transition ratios (V2/V1) were linearly dependent on the narrow-to-wide structures ($D1/D2 < 1$). In contrast, the wide-to-narrow structures ($D1/D2 > 1$) did not show apparent correlations except for the general acceleration tendency when entering the narrow region.

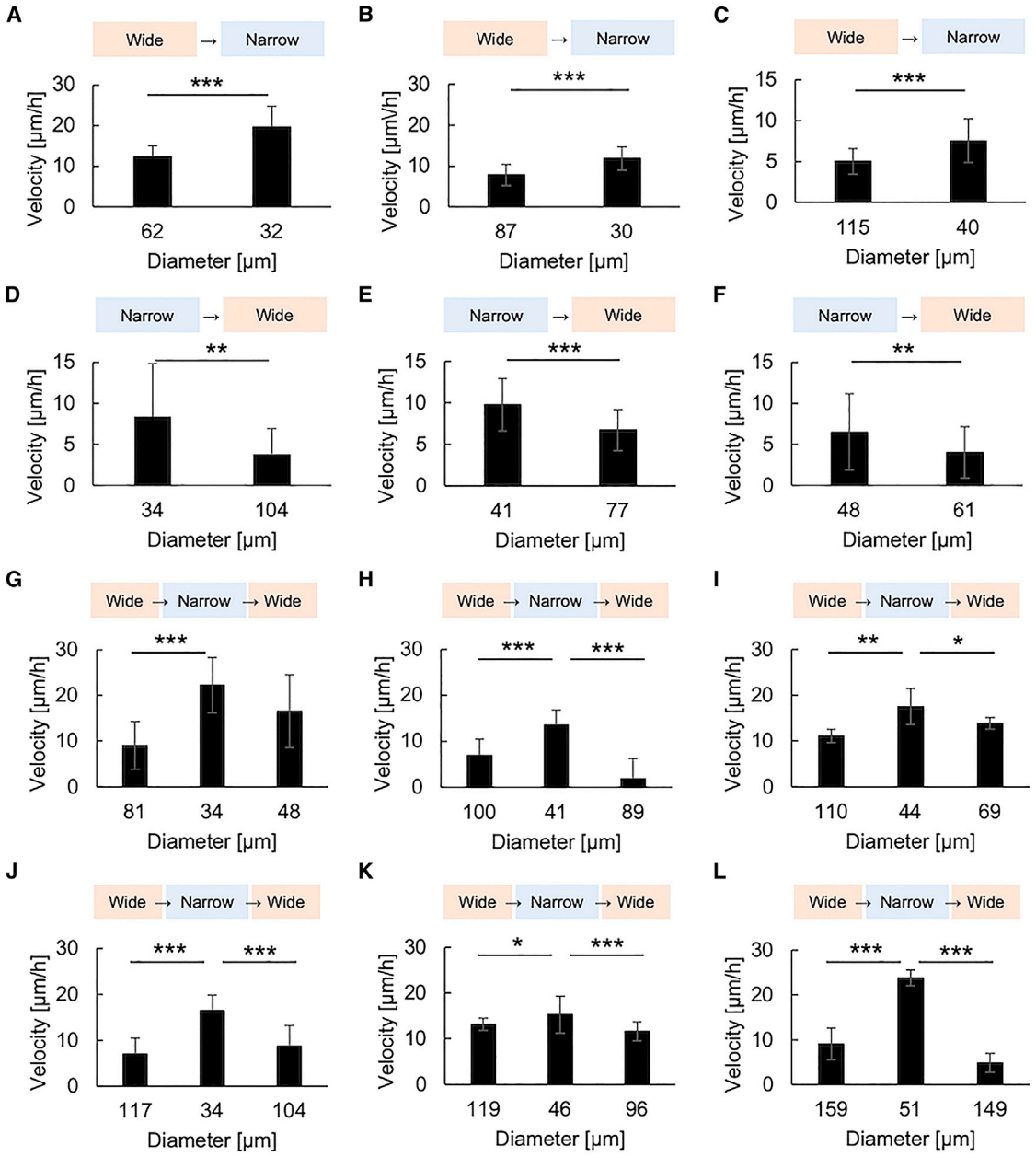

FIGURE 4 Histograms demonstrating the results of the significance tests between the collective migration velocity of sequential regions with varying diameters. The dataset was first examined with the Shapiro-Wilk test to distinguish whether the data were following the normal distribution. For parametric data set, F test was used to analyze the variance, followed with either a Student t test or Welch t test depending on whether the null hypothesis was rejected (*G*, *I*, and *K*). For non-parametric data, Mann-Whitney U test was employed to compare the data set (*A*–*F*, *H*, *J*, and *L*). (*A*), (*D*), and (*J*) are adopted from Fig. 3 *N*, *O*, and *P*, respectively. *$p < 0.05$, **$p < 0.01$, ***$p < 0.001$.

DISCUSSION

This study examined the contribution of geometric factors to the collective cell migration behavior in 3D borderless sheet structures. We have newly developed the flexible 3D microtunnel fabrication technology exploiting the gelatin gel with photo-thermal etching technology. Utilizing this technology, the combined adjustable sizes of straight channels were formed successfully. Significantly, the wide-narrow-wide structures in the straight tunnels have not been fabricated by the conventional cast-mold approaches. We applied these flexible 3D gelatin microtunnel structures to examine the dominant geometric factors of collective cell migration in the 3D designs. The confinement size dependency of collective cell migration velocity under diameter-changing microtunnel structures was observed. By sequentially altering the diameter within

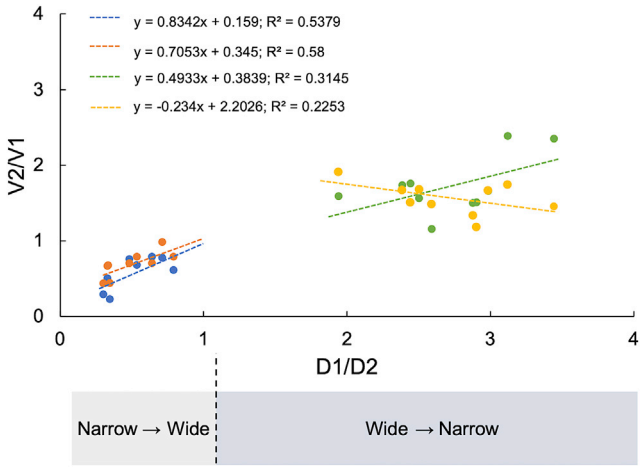

FIGURE 5 Correlation between the subsequent velocity changes and the diameter changes of the microtunnel. Analysis of the correlation between the ratio of the microtunnel size change and the ratio of the corresponding velocity change. D1, V1 (inlet side), and D2, V2 (outlet side) are diameters and migration velocities before and after structural changes, respectively. Orange and yellow circles represent the comparison between the maximum peak velocity change ratio (V2/V1) of two consecutive tunnels having a diameter change ratio (D1/D2), and the blue and green circles are the relation between the average velocity ratio (V2/V1) and the diameter ratio. The blue and orange least-squares regression lines exhibited a strong correlation when the diameter change ratio was lower than 1, indicating that the transition from narrow to wide regions of the microstructure satisfied the continuity equation. On the other hand, the tendency is weaker for the diameter ratios above 1, during the transition from wide to narrow regions.

the microtunnel, the influence of cell supply on collective cell migration velocity was corroborated, especially by the wide-narrow-wide platform.

Here, we employed a chemical approach using glutaraldehyde as the crosslinking agent of the gelatin gel. While glutaraldehyde itself is toxic to the cells, thoroughly washing the residual glutaraldehyde and non-cross-linked gelatin with water prior to cell seeding allowed for a viable culturing platform. As a derivative of collagen that pertains to similar molecular structure and function, gelatin has been used as a replacement biomaterial due to its cost-effectiveness, biocompatibility, and intrinsic cell adhesion motifs that eliminate the need for coating with ECM proteins (43,44). In addition, previous records have reported successful cultivation of bovine coronary ECs (45) and human mesenchymal stem cells (46) on glutaraldehyde-cross-linked gelatin gel. Furthermore, other crosslinking methods using an enzymatic approach and bio-orthogonal strategies have confirmed similar cellular responses and practicability as a culturing environment for different types of cells, including cardiomyocytes (47) and human dental pulp stem cells (48). Thus, the technology to microfabricate 3D structures inside the gelatin gel offer a cost-effective and facilitated method for the preparation of a cell culturing environment that mimics a physiologically relevant tissue formation system.

The microtunnels fabricated inside the gelatin-hydrogel cube ranged between 30 and 160 μm. The range of the diameter adopted here mimics the dimensions of the physiological structures of blood vessels such as arterioles and venules that have a typical diameter between 10 to 100 μm, and the smaller arteries and veins that have the diameters of 100 μm to 10 mm and 100 μm to 100 mm, respectively (49,50). The inner layers of these blood vessels are composed of endothelium, which also justifies the reason for using ECs in this experiment (51).

Through observing collective cell behavior inside an altered-diameter microtunnel, we have observed how these cells respond to the physical changes in the environment. As shown in Fig. 5, a concrete relationship between the ratio of diameter change of microtunnels and the ratio of propagation velocity in narrow-wide structures supports the idea that collective cell migration responded in programmed ways when reducing cell-cell interactions as the cells infiltrate to a wider region. Physiologically, especially in embryo development, the precise positioning of particular cells enables the formation of tissues and organ progenitors during their movement in groups. Even after birth, accurate control of positions of cells shape organs and drives wound healing. These examples suggest that living tissues respond in programmed ways to environmental cues. For example, polygonal shapes of deformable cells in epithelial monolayers were well explained by the optimization of total areas and perimeters of whole component cells in the tissue, and, moreover, cells can acquire fluid-like behavior by increasing the cell perimeter-to-area ratio in one of two ways, either decreasing intracellular tension or increasing cell-to-cell adhesion (20,52,53). In contrast, our results also indicate that the change of physical confinement that accumulates cell-to-cell interactions in wide-narrow structures induces a more uncertain response to environmental changes and hence might reduce the ability of precise positioning and shape formation of each cell by the loss of controlling geometric regulation, which is required for the programmed behavior.

A previous report showed that the collective cell migration velocity in 3D capillary structure was regulated by its diameter at least in the 30–160 μm range (32,54). However, the microtunnels fabricated here resulting in the same range of sizes showed that the diameter size did not dominate their migration velocity. This could be due to the difference in extracellular matrix or the inconsistency of cell source prior to microtunnel invasion. Still, the density of supplied cells is the primary

contributor to the propagation velocities of cell sheets to conserve the cell density constant. This signifies that the narrowing of the inner diameter of the tube should accelerate the propagation velocity, and the widening of the inner diameter of the tube should cause deceleration to the propagation velocity to satisfy the continuity equation. In other words, the migration velocity should be regulated to maintain the cell density constant. Because the results of the narrow-wide change in Fig. 5 showed an apparent direct proportion between the microtunnel diameter change (or the circumference length change) and migration velocity change, this transition obeys the expected conservation of cells and velocity. In contrast, the narrowing patterns did not show a direct proportion tendency but just an acceleration of their migration velocity. This may be explained by the difference in the sensitivity to the external cues of the regulated cell-to-cell interaction. The sudden widening has no restricting factor other than the simple interaction reduction between the proximity cell as the cells leave the narrow region. However, for the wide-narrow transition, cells accumulate and cause compression of the cells at the entrance, which prohibits a smooth transition into the narrower part, which is inherently different from ordinary matters. Hence, the cells may experience opposing forces from the geometry, limiting the sensitivity to accelerate according to the size constriction of the environment.

A large fluctuation of the propagation velocity of collective migration was observed even in the straight 3D mictrotunnel structures (Fig. 2). However, similar large fluctuations were reported in 2D stripe structures (6,42). Recently, the existence of periodical stress gradients caused by the feedback control of combined mechanical waves and chemical waves of extracellular signaling molecule in cell sheets were reported (55). Assuming that cells polarize in different forms in response to local stress gradients in the confined structures, the fluctuation or rather oscillation of propagation velocity might be appropriate.

This paper introduced a new method of flexible design of 3D structures in gelatin gel. By altering the diameter of the tubular shapes, we showed one of the advantages of this assay by comparing the propagation manner during the environmental changes under the same cell supply condition. We speculate that the full picture of collective cell migration itself is still uncertain in this experiment. More detailed insights into the cell migration velocity rule should be examined in the complimentary 2D model within the flexible changed channel model. Stable cell supply to the inlet of the microtunnel is another issue to be improved. One reason for the fluctuating collective cell migration velocity should be the dispersion of cell numbers at the entrance of microtunnels. There remains the possibility that this fluctuation is the nature of collective cell migration on the inner surface of the cylindrical 3D capillary structures. However, improvements are required for this assay to have a stable cell supply reservoir connected to the inlets of microtunnels.

The capability and limitation of microfabrication size is another technological issue for considering potential applications. This microfabrication technology is achieved by manipulating the heat spot of laser absorption at the tip of the platinum-coated microneedle. Thereby, creating a structure with varying dimensions is made possible. The strength of this technology resides in the ease of preparation of a confined culturing platform. Compared with the conventional PDMS method, which revolves around the cast-molding method, the user has flexible control over the structure's dimension of interest during the microfabrication process. During this investigation, microtunnels with inner diameters of approximately 30–160 μm were formed. However, this confinement size can be made even smaller/larger in our technology by controlling the parameters such as needle tip size, laser intensity, and microscope magnification, and by using different materials with better thermal emissivity/absorptivity for metal deposition on the needle. In practice, for the preparation of a 2D culturing platform, we have improved our photo-thermal agarose microfabrication technology and accomplished fabricating structures smaller than the applied infrared laser wavelength using the absorption of a 0.7-μm microneedle, as absorption itself is independent of the wavelength-dependent diffraction limit of the condensing objective lens (56). Moreover, we have developed another spot heating technology for agarose microfabrication with joule heat of microionic current at the tip of the 0.3-μm microcapillary tube (57). Despite being able to regulate the size of the microtunnels, only unidirectional tubular confinements are possible, and diverse patterns available for 2D culturing environments cannot be fabricated with this technology yet. Overcoming these limits should be the next step in our challenge to improve the system for a more versatile 3D microfabrication assay to prepare a more in vivo-like platform for assessing cellular dynamics.

CONCLUSIONS

We have developed a method to fabricate the flexible 3D structures of capillary microtunnels to examine the collective movement behavior of the borderless cylindrical vascular EC sheet during the flexible change of tube structures. The results showed that 1)ECs moved and spread two-dimensionally on the inner surface of capillary microtunnels as a monolayer instead of filling the entire capillary, 2) the inlet diameter of

microtunnels does not determine the maximum peak migration velocity, 3) the change ratio of collective migration velocity of borderless cylindrical cell sheet in the narrow-to-wide microtunnel is in direct proportion to the increase ratio of circumference length of the tunnel, and 4) those in the wide-to-narrow change accelerated the migration speed but no apparent correlation between the change ratio of velocity and that of circumference length change was observed. In conclusion, those results demonstrate the ability of the flexible 3D fabrication technology, and indicate that the migration velocity of the borderless cylindrical cell sheet responds to the change of circumference length and emerged migratory modes for epithelial migration under flexible 3D confinement as fluid flow-like behavior with conservation of cell numbers.

AUTHOR CONTRIBUTIONS

K.Y. conceived the experiments. M.S., H.H., and K.I. conducted the experiments. M.S., H.H., K.I., and K.Y. analyzed the results. M.S., H.H., K.I., and K.Y. wrote the draft and final version of the manuscript. All authors reviewed the manuscript.

ACKNOWLEDGMENTS

We thank Dr. Akihiro Hattori, Mr. Masao Odaka, and all the members of the Yasuda laboratory for their technical support, discussion, and suggestions. This research was funded by research and development projects of the Industrial Science and Technology Program, the New Energy and Industrial Technology Development Organization (NEDO, P08030), JSPS KAKENHI grant (JP17H02757), JST CREST program (1J138), and Waseda University Grant for Special Research Projects (2016S-093, 2017B-205, 2017K-239, 2018K-265, 2018B-186, 2019C-559, 2020C-276, 2021C-572, 2022C-143), the Leading Graduate Program in Science and Engineering for Waseda University from MEXT, Japan.

DECLARATION OF INTERESTS

The authors declare no competing interests.

REFERENCES

1. Friedl, P., and D. Gilmour. 2009. Collective cell migration in morphogenesis, regeneration and cancer. *Nat. Rev. Mol. Cell Biol.* 10:445–457.
2. Rørth, P. 2009. Collective cell migration. *Annu. Rev. Cell Dev. Biol.* 25:407–429.
3. Gillespie, P. G., and R. G. Walker. 2001. Molecular basis of mechanosensory transduction. *Nature.* 413:194–202.
4. Alert, R., and X. Trepat. 2020. Physical models of collective cell migration. *Annu. Rev. Condens. Matter Phys.* 11:77–101.
5. Garcia, S., E. Hannezo, …, N. S. Gov. 2015. Physics of active jamming during collective cellular motion in a monolayer. *Proc. Natl. Acad. Sci. USA.* 112:15314–15319.
6. Marel, A. K., M. Zorn, …, J. O. Rädler. 2014. Flow and diffusion in channel-guided cell migration. *Biophys. J.* 107:1054–1064.
7. Vedula, S. R. K., M. C. Leong, …, B. Ladoux. 2012. Emerging modes of collective cell migration induced by geometrical constraints. *Proc. Natl. Acad. Sci. USA.* 109:12974–12979.
8. Scarpa, E., and R. Mayor. 2016. Collective cell migration in development. *J. Cell Biol.* 212:143–155.
9. Vasilyev, A., Y. Liu, …, I. A. Drummond. 2009. Collective cell migration drives morphogenesis of the kidney nephron. *PLoS Biol.* 7:e1000009.
10. Nnetu, K. D., M. Knorr, …, M. Zink. 2012. The impact of jamming on boundaries of collectively moving weak-interacting cells. *New J. Phys.* 14:115012.
11. Ilina, O., and P. Friedl. 2009. Mechanisms of collective cell migration at a glance. *J. Cell Sci.* 122:3203–3208.
12. Shaw, T. J., and P. Martin. 2009. Wound repair at a glance. *J. Cell Sci.* 122:3209–3213.
13. Geudens, I., and H. Gerhardt. 2011. Coordinating cell behaviour during blood vessel formation. *Development.* 138:4569–4583.
14. Friedl, P., J. Locker, …, J. E. Segall. 2012. Classifying collective cancer cell invasion. *Nat. Cell Biol.* 14:777–783.
15. Ishida, S., R. Tanaka, …, H. Haga. 2014. Epithelial sheet folding induces lumen formation by Madin-Darby canine kidney cells in a collagen gel. *PLoS One.* 9:e99655.
16. Ewald, A. J., A. Brenot, …, Z. Werb. 2008. Collective epithelial migration and cell rearrangements drive mammary branching morphogenesis. *Dev. Cell.* 14:570–581.
17. Andrew, D. J., and A. J. Ewald. 2010. Morphogenesis of epithelial tubes: Insights into tube formation, elongation, and elaboration. *Dev. Biol.* 341:34–55.
18. Lubarsky, B., and M. A. Krasnow. 2003. Tube morphogenesis: Making and shaping biological tubes. *Cell.* 112:19–28.
19. Bi, D., X. Yang, …, M. L. Manning. 2016. Motility-driven glass and jamming transitions in biological tissues. *Phys. Rev. X.* 6:021011.
20. Bi, D., J. H. Lopez, …, M. L. Manning. 2015. A density-independent rigidity transition in biological tissues. *Nat. Phys.* 11:1074–1079.
21. Mazalan, M. B., M. A. B. Ramlan, …, T. Ohashi. 2020. Effect of geometric curvature on collective cell migration in tortuous microchannel devices. *Micromachines.* 11:659.
22. Callens, S. J. P., R. J. C. Uyttendaele, …, A. A. Zadpoor. 2020. Substrate curvature as a cue to guide spatiotemporal cell and tissue organization. *Biomaterials.* 232:119739.
23. Brückner, D. B., A. Fink, …, C. P. Broedersz. 2019. Stochastic nonlinear dynamics of confined cell migration in two-state systems. *Nat. Phys.* 15:595–601.
24. Park, J., D. H. Kim, and A. Levchenko. 2018. Topotaxis: A new mechanism of directed cell migration in topographic ECM gradients. *Biophys. J.* 114:1257–1263.
25. Kim, J., Y. Zheng, …, B. Sun. 2020. Geometric dependence of 3D collective cancer invasion. *Biophys. J.* 118:1177–1182.
26. Paul, C. D., W.-C. Hung, …, K. Konstantopoulos. 2016. Engineered models of confined cell migration. *Annu. Rev. Biomed. Eng.* 18:159–180.
27. Montesano, R., L. Orci, and P. Vassalli. 1983. In vitro rapid organization of endothelial cells into capillary-like networks is promoted by collagen matrices. *J. Cell Biol.* 97:1648–1652.
28. Montesano, R., G. Schaller, and L. Orci. 1991. Induction of epithelial tubular morphogenesis in vitro by fibroblast-derived soluble factors. *Cell.* 66:697–711.
29. Montesano, R., K. Matsumoto, …, L. Orci. 1991. Identification of a fibroblast-derived epithelial morphogen as hepatocyte growth factor. *Cell.* 67:901–908.
30. Yevick, H. G., G. Duclos, …, P. Silberzan. 2015. Architecture and migration of an epithelium on a cylindrical wire. *Proc. Natl. Acad. Sci. USA.* 112:5944–5949.

31. Ye, M., H. M. Sanchez, …, P. C. Searson. 2014. Brain microvascular endothelial cells resist elongation due to curvature and shear stress. *Sci. Rep.* 4:4681.
32. Xi, W., S. Sonam, …, C. Teck Lim. 2017. Emergent patterns of collective cell migration under tubular confinement. *Nat. Commun.* 8:1517.
33. Costa, P. F., H. J. Albers, …, A. D. van der Meer. 2017. Mimicking arterial thrombosis in a 3D-printed microfluidic: In vitro vascular model based on computed tomography angiography data. *Lab Chip.* 17:2785–2792.
34. Sentoku, M., H. Hashimoto, …, K. Yasuda. 2021. Photothermal agarose microfabrication technology for collective cell migration analysis. *Micromachines.* 12:1015.
35. Reffay, M., L. Petitjean, …, P. Silberzan. 2011. Orientation and polarity in collectively migrating cell structures: Statics and dynamics. *Biophys. J.* 100:2566–2575.
36. Petitjean, L., M. Reffay, …, P. Silberzan. 2010. Velocity fields in a collectively migrating epithelium. *Biophys. J.* 98:1790–1800.
37. Mark, S., R. Shlomovitz, …, P. Silberzan. 2010. Physical model of the dynamic instability in an expanding cell culture. *Biophys. J.* 98:361–370.
38. Poujade, M., E. Grasland-Mongrain, …, P. Silberzan. 2007. Collective migration of an epithelial monolayer in response to a model wound. *Proc. Natl. Acad. Sci. USA.* 104:15988–15993.
39. Endresen, K. D., M. Kim, …, F. Serra. 2021. Topological defects of integer charge in cell monolayers. *Soft Matter.* 17:5878–5887.
40. Blanch-Mercader, C., V. Yashunsky, …, P. Silberzan. 2018. Turbulent dynamics of epithelial cell cultures. *Phys. Rev. Lett.* 120:208101.
41. Saw, T. B., A. Doostmohammadi, …, B. Ladoux. 2017. Topological defects in epithelia govern cell death and extrusion. *Nature.* 544:212–216.
42. Duclos, G., C. Blanch-Mercader, …, P. Silberzan. 2018. Spontaneous shear flow in confined cellular nematics. *Nat. Phys.* 14:728–732.
43. Bello, A. B., D. Kim, …, S.-H. Lee. 2020. Engineering and functionalization of gelatin biomaterials: From cell culture to medical applications. *Tissue Eng. Part B Rev.* 26:164–180.
44. Selestina, G., and K. Vanja. 2011. Collagen- vs. gelatine-based biomaterials and their biocompatibility: Review and perspectives. *In* Biomaterials Applications for Nanomedicine. R. Pignatello, ed. IntechOpen, pp. 17–52.
45. Ai, H., D. K. Mills, …, S. A. Jones. 2002. Gelatin-glutaraldehyde cross-linking on silicone rubber to increase endothelial cell adhesion and growth. *In Vitro Cell. Dev. Biol. Anim.* 38:487–492.
46. Yang, L. J., and Y. C. Ou. 2005. The micro patterning of glutaraldehyde (GA)-crosslinked gelatin and its application to cell-culture. *Lab Chip.* 5:979–984.
47. Tijore, A., S. A. Irvine, …, S. Venkatraman. 2018. Contact guidance for cardiac tissue engineering using 3D bioprinted gelatin patterned hydrogel. *Biofabrication.* 10:025003.
48. Contessi Negrini, N., A. Angelova Volponi, …, A. D. Celiz. 2021. Tunable cross-linking and adhesion of gelatin hydrogels via bioorthogonal click chemistry. *ACS Biomater. Sci. Eng.* 7:4330–4346.
49. Burton, A. C. 1954. Relation of structure to function of the tissues of the wall of blood vessels. *Physiol. Rev.* 34:619–642.
50. Schöneberg, J., F. De Lorenzi, …, H. Fischer. 2018. Engineering biofunctional in vitro vessel models using a multilayer bioprinting technique. *Sci. Rep.* 8:10430.
51. Cao, X., S. Maharjan, …, Y. S. Zhang. 2021. Bioprinting of small-diameter blood vessels. *Engineering.* 7:832–844.
52. Park, J. A., J. H. Kim, …, J. J. Fredberg. 2015. Unjamming and cell shape in the asthmatic airway epithelium. *Nat. Mater.* 14:1040–1048.
53. Farhadifar, R., J. C. Röper, …, F. Jülicher. 2007. The influence of cell mechanics, cell-cell interactions, and proliferation on epithelial packing. *Curr. Biol.* 17:2095–2104.
54. Xi, W., S. Sonam, …, B. Ladoux. 2018. Tubular microscaffolds for studying collective cell migration. *Methods Cell Biol.* 146:3–21.
55. Boocock, D., N. Hino, …, E. Hannezo. 2021. Theory of mechanochemical patterning and optimal migration in cell monolayers. *Nat. Phys.* 17:267–274.
56. Tanaka, Y., H. Watanabe, …, K. Yasuda. 2021. Stepwise neuronal network pattern formation in agarose gel during cultivation using non-destructive microneedle photothermal microfabrication. *Sci. Rep.* 11:18197.
57. Shimoda, K., H. Watanabe, …, K. Yasuda. 2022. In situ agarose microfabrication technology using Joule heating of micro ionic current for on-chip cell network analysis. *Micromachines.* 13:174.